Published in final edited form as:
Macromolecules. 2012 June 12; 45(11): 4896–4906. doi:10.1021/ma3004778.

The Structure of Hydrated Poly (D, L - Lactic Acid) Studied With X-Ray Diffraction and Molecular Simulation Methods

Xianfeng Li[†], **N. Sanjeeva Murthy**[‡], and **Robert A. Latour**[†,*]

[†]Department of Bioengineering, Clemson University, Clemson, South Carolina 29634, United States

[‡]New Jersey Center for Biomaterials, Rutgers University, Piscataway, New Jersey 08854, United States

Abstract

The effect of hydration on the molecular structure of amorphous poly (D, L-lactic acid) (PDLLA) with 50:50 L-to-D ratio has been studied by combining experiments with molecular simulations. X-ray diffraction measurements revealed significant changes upon hydration in the structure functions of the copolymer. Large changes in the structure functions at ~ 10 days of incubation coincided with the large increase in the water uptake from ~1 to ~40% and the formation of voids in the film. Computer modeling based on the recently developed TIGER2/TIGER3 mixed sampling scheme was used to interpret these changes by efficiently equilibrating both dry and hydrated models of PDLLA. Realistic models of bulk amorphous PDLLA structure were generated as demonstrated by close agreement between the calculated and the experimental structure functions. These molecular simulations were used to identify the interactions between water and the polymer at the atomic level including the change of positional order between atoms in the polymer due to hydration. Changes in the partial O-O structure functions, about 95% of which were due to water-polymer interactions, were apparent in the radial distribution functions. These changes, and somewhat smaller changes in the C-C and C-O partial structure functions, clearly demonstrated the ability of the model to capture the hydrogen bonding interactions between water and the polymer, with the probability of water forming hydrogen bonds with the carbonyl oxygen of the ester group being about four times higher than with its ether oxygen.

1. Introduction

Currently there is great interest in hydrolytically degradable polymers for drug delivery, tissue engineering, and regenerative medicine applications.[1–6] Their physical and mechanical properties and service life are greatly influenced by the effects of moisture, either in the form of humidity or by immersion in water. A rational design of these polymers for intended applications requires a fundamental understanding of the mechanisms that contribute to their hydrolytic degradation, which is influenced by the absorption and distribution of water within the polymer and its subsequent effects on polymer structure and hydrolysis at the molecular level.

Polylactic acid (PLA), or polylactide, is an important type of hydrolytically biodegradable aliphatic polyester. It has two optical isomers, i.e. L-lactic acid [(S)-2-hydroxypropanoic acid] and its mirror image D-lactic [(R)-2-hydroxypropanoic acid].[7] The structure of PLA composed of L-lactic and D-lactic units (PDLLA) depends on the ratio of L- to D- lactic acid units. For example, if the L:D (or D:L) ratio is more than 78:22, PDLLA typically

*To whom all correspondence should be addressed. latourr@ces.clemson.edu.

solidifies in a semicrystalline state, whereas a lower ratio leads to amorphous state.[8–10] In this work, the amorphous PDLLA with 50:50 L:D lactide monomer ratio was studied. Its structure change due to hydration was investigated by synergistically combining experiments with molecular simulations. In experiments, the structural changes caused by hydration at the molecular length scale were studied using wide-angle x-ray diffraction (WAXD). Since the polymers that were studied are amorphous, WAXD data can be analyzed using pair-distribution functions (PDFs) and structure factors. The computer simulation with carefully constructed atomic models of the polymer is able to help further extract the causes that lead to the change of the structure factor reported by experiment and provides detailed information on the dynamics of the hydrating water molecules, the interactions between the water molecules and the polymer, and the formation of water clusters around the various functional groups of the polymer.

For amorphous PDLLA composed of densely packed, randomly entangled chains, it is challenging for computer modeling to establish representative models of equilibrated structures in dry and wet states. Up to now, there are only a few papers published regarding modeling hydration or degradation processes in PLA.[11–15] These previous simulations were conducted by using classical molecular dynamics (MD) methods to equilibrate the dry structure represented by all-atom models and represent the partitioning of water molecules within the polymer. However, the classical MD method is well known to be very inefficient for the treatment of dense polymer systems due to chain entanglement issues and these previous studies were very limited because of the small size of systems that were modeled. We recently developed a systematic sampling scheme[16–19] to effectively accelerate the equilibration of bulk-phase models of amorphous polymers. The scheme consists of three parts: (1) coarse graining the atomistic model of the amorphous polymer to reduce the number of the degrees of freedom in the system, (2) accelerating the sampling with a mixed sampling scheme of the “temperature intervals with global exchange of replicas” (TIGER2) method[17, 18] and the “temperature intervals with global exchange of replicas and reduced radii” (TIGER3) method,[16] and (3) re-constructing the atomic model by a reverse-mapping method.[19] In the coarse graining method to map an atomistic model onto a CG model, several atoms are grouped together into a relatively simple “super-atom assembly” (or CG bead) and the interaction energies between respective CG beads are obtained by the application of an optimization procedure that reproduces the structural distributions obtained from atomistic simulations.[20–25] A CG model keeps the description of microscopic properties at the necessary level of accuracy and detail but can greatly speed up the equilibration procedure. Both TIGER2 and TIGER3 methods conduct a number of parallel molecular dynamics simulations at different temperature levels. The replica at the baseline temperature goes through regular molecular dynamics while the replicas at temperatures above the baseline go through a series of cycles with each cycle consisting of heating, sampling, quenching, and temperature level reassignment. The TIGER2 method enables the system to rapidly escape from local energy minima and the TIGER3 method eliminates the entanglement among chain segments by providing a mechanism for polymer chains to pass through one another during the simulation. The ability of the TIGER2/TIGER3 scheme to generate well–equilibrated molecular models of dense-phase amorphous polymer structures was introduced in ref. 16. In the present work, TIGER2/TIGER3 was applied to equilibrate the structures of dry and hydrated PDLLA. The calculated structures were then examined by comparing the structure factor with the corresponding experimental results, with the molecular structure of the copolymer further analyzed to provide insight into the experimental observations.

2. Methodology

This section introduces the methods used in the present work, including the experimental methods in measuring hydration, degradation, and structure functions of dry and hydrated PDLLA samples, details of the TIGER2/TIGER3 algorithm, the modeling approach used to develop CG parameters for the PDLLA copolymer, and the setup of the simulations that were conducted to construct structural models of PDLLA in dry and hydrated states.

2.1. The Experimental Method

2.1.1. Hydration and Degradation—PDLLA was obtained from Sigma-Aldrich (inherent viscosity 0.55–0.75 dL/g). The molecular weight (M_w) determined by gel permeation chromatography (GPC) in tetrahydrofuran (calibrated using polystyrene standards) was ~ 96,000 Da. Films, ~200 μm in thickness, were compression molded in a Carver press. Samples (6.0 mm in diameter) punched out of these films were incubated at 37 °C in phosphate buffered saline (PBS). Samples were evaluated at various time points for up to 70 days of immersion. Water content was determined both by weighing the dry and hydrated samples, as well as by measuring the weight loss between 30 and 130 °C. Degradation was followed by monitoring the changes in molecular weight at various time points using GPC.

2.1.2. X-Ray Scattering—The structure functions of PDLLA samples in dry and wet states were obtained from the x-ray scattering curves measured from q= 0.3 to 20 $Å^{-1}$ on the beam line 11-ID-C at the Advanced photon source (APS), Argonne National Laboratory, Argonne, IL (USA). q is the scattering vector defined as $(4\pi \sin\theta)/\lambda$, where 2θ is the scattering angle and λ is the x-ray wavelength. Samples were inserted into 2.0 mm diameter x-ray quartz capillaries, and data were collected in transmission geometry at ambient temperature. The x-ray beam from a Si(311) Laue monochromator (115 keV, λ = 0.1078 Å) was collimated to a beam size of about 0.2×0.2 mm. Diffraction patterns were collected using a Perkin Elmer amorphous Silicon 1621 AN3 detector with 10 min exposure (5 s/frame, 24 frames/file and 5 files/data set). The background was measured using an empty 2.0 mm quartz capillary for subsequent subtraction from the sample scattering curves. The raw data were integrated and converted to intensity versus scattering wave vector, q, using the Fit2D software.[26] Six sharp spikes in the data between q = 6 and 9 $Å^{-1}$ due to the detector were removed by interpolation of points on either side of these spikes. The observed coherent x-ray scattering intensity, $I_{coh}(q)$, was used to derive structure function $S(q)$ defined as:

$$S(q)=\frac{I_{coh}(q)-\sum_i x_i f_i^2(q)}{\left[\sum_i x_i f_i(q)\right]^2}, \quad (1)$$

where for atomic species i, x_i and f_i are the atomic fraction and x-ray form factor, respectively. The program PDFgetX2 [27] was used to obtain the total scattering function $S(q)$ after corrections for sample absorption, Compton scattering and multiple scattering. Because of the high energy of the x-rays and the transmission geometry used for these measurements, the corrections for sample absorption and multiple scattering are negligible.

2.2. The TIGER2/TIGER3 Sampling Scheme

In the combined TIGER2/TIGER3 sampling scheme,[16] a TIGER2 process is composed of a number of replicas of the molecular system (N_r). The replica at baseline temperature (T_B)

undergoes sampling via regular molecular dynamics while the rest of replicas are conducted through a series of sampling cycles with each cycle containing four stages: (1) rapid heating from T_B to the designated elevated temperature (T_m) by rescaling the momenta of the atoms within the replica by a factor of $\sqrt{T_m/T_B}$ followed by thermal equilibration, (2) molecular dynamics sampling at the constant elevated temperature level (T_m), (3) rapid quenching back down to T_B by rescaling the momenta by a factor of $\sqrt{T_B/T_m}$ followed by thermal equilibration, and (4) global replica reassignment. Stage (4) consists of two substeps: (*i*) one state from among the set of (N_r – 1) quenched states is randomly selected, and the potential energy of this state is then compared with the state from the production run of the baseline replica using the Metropolis importance sampling criterion,[28] and (*ii*) all replicas except the selected baseline replica are then reassigned to the higher temperature levels according to their potential energies; i.e., a higher potential energy state is assigned to a higher temperature level. The strategy of how to determine the length of each stage in a TIGER2 cycle has been studied in ref. 18, which determined that the proper lengths for heating, sampling, and quenching are about 1 – 2 ps, 4 – 6ps, and 2 – 4ps, respectively. A TIGER3 process is similar to that of TIGER2 in cycling. The only difference of TIGER3 from TIGER2 is that, in TIGER3, the sampling stage at elevated temperature levels is conducted with four substeps under constant volume conditions composed of (1) Monte Carlo (MC) sampling with reduced VDW radii (we used zero VDW radii to turn off both attraction and repulsion terms), (2) energy minimization with the VDW radii recovered to their regular force field values, (3) relaxation using the MC method, and (4) molecular dynamics sampling for further equilibration. A schematic illustrating the TIGER2/TIGER3 algorithm is shown by Figure 1. The ratio of TIGER2 to TIGER3 cycles implemented in the mixed method was determined by the value of the exchange acceptance ratio that was obtained from a pre-test run. We found that the pre-test runs with one TIGER3 cycle for every ten TIGER2 cycles provided about 30% exchange acceptance ratio, and thus a 10: 1 ratio of TIGER2 to TIGER3 cycles was selected in all simulations in this work.

All simulations were carried out with the CHARMM program[29, 30] using the Nose-Hoover thermostat[31–33] for constant volume and constant temperature. For atomic model calculations, the SHAKE algorithm[29] was used to constrain all bond lengths containing hydrogen. The velocity-Verlet algorithm[29, 34] was used with a time step of 1 fs to integrate the equations of motion in the dynamics simulations. All simulations were performed with an atom-based 14 Å cutoff. In the 10:1 TIGER2/TIGER3 scheme, each TIGER2 cycle contained a sequence of 2 ps heating, 4 ps sampling, and 4 ps quenching and relaxation processes and each TIGER3 cycle included similar heating and quenching processes as those in TIGER2, but with the implementation of the above-described substeps at each elevated temperature, which were composed of: (1) 10^5 steps of MC sampling for the dihedral angles conducted with zero VDW radii, (2) energy minimization with recovered VDW radii conducted with 500 steps of steepest descent (SD) method followed by another 500 steps of adopted basis Newton – Raphson (ABNR) method,[29] (3) 10^5 steps of MC sampling for the dihedral angles and atom positions, and (4) 4 ps molecular dynamics sampling. All simulations used eight replicas at evenly spaced temperature levels. The temperature difference between successive levels is typically set to be between 40–50 K.[18]

2.3. Coarse – Grained Model of PDLLA

The coarse graining force field was developed using the CHARMM molecular simulation package internally adapted by our group to use the polymer consistent force field (PCFF),[35–38] in which the all-atom model total force field energy (E) is calculated by

$$E = E_{bonded} + E_{non-bonded}, \quad (2)$$

where E_{bonded} and $E_{non\text{-}bonded}$ are bonded and non-bonded potential terms, respectively. These terms are decomposed as,

$$E_{bonded} = E_{stretch} + E_{bend} + E_{torsion} + E_{cross}$$
$$E_{non-bonded} = E_{VDW} + E_{Coulomb}, \quad (3)$$

where $E_{stretch}$, E_{bend} and $E_{torsion}$ are the bond-length-stretching, angle-bending, and bond-rotation energies, respectively; the cross term, E_{cross}, accounts for the coupling between individual bonded interactions; E_{VDW} accounts for the excluded volume repulsive as well as the intermolecular attractive forces between non-bonded atoms; and $E_{Coulomb}$ is the electrostatic potential. In developing the CG model of PDLLA, the E_{cross} term was not considered and the electrostatic interactions between non-bonded super-atoms were reasonably ignored since all CG beads were constructed to be net-neutral. Therefore, the potential terms that need to be parameterized included $E_{stretch}$, E_{bend}, $E_{torsion}$, and E_{VDW}. For each term, CG parameterization was conducted based on the iterative Boltzmann inversion of the corresponding atomistic distribution functions. Following our previous work,[16, 19] the distributions of bond lengths and bond angles were fitted by a double Gaussian function and the distributions of dihedral angles were fitted by three-fold Fourier progression forms. The parameterization of the VDW interactions was conducted by matching the radial distribution functions (RDF) obtained by the CG model and the atomistic model for compounds that have similar atomic structure assigned in a CG bead.

The atomic structure of D-lactic acid or L-lactic acid unit in the PDLLA chain is given in Figure 2. In the coarse graining process, each D-lactic acid or L-lactic acid monomer was treated as a single bead, represented by D or L, and the mapping point was taken as the center of mass of each bead. The presence of different types of CG beads in the polymer introduces new CG potentials. All possible compositions of CG bonds, bond angles, and dihedral angles in a PDLLA chain are summarized in Table S1 in supplementary materials.

The CG parameters for bonded interactions were obtained by first conducting atomistic simulations using the TIGER2 sampling method for ten types of single hexamer (each contains six repeat units), i.e., E1DDDDE2, E1DDDLE2, E1DDLDE2, E1DDLLE2, E1DLDLE2, E1DLLDE2, E1LDDLE2, E1DLLLE2, E1LDLLE2, and E1LLLLE2, in which the chains are ended with E1 = $CH_2CH_3COO–$ and E2 = $–CHCH_3COOH$. The modified PCFF parameters[39] for dihedral angles centered by C-C and C-O bonds were used in the atomic simulations to obtain target distributions of bond length, bond angle and dihedral angle. Starting from extended conformations, the ten polymer hexamers were equilibrated in a period box with dimensions 16.85 × 16.85 × 16.85 $Å^3$, which was set to provide similar density to amorphous PDLLA (1.25 g/cm^3). The equilibration was conducted with the TIGER2 method using eight replicas at evenly spaced temperature levels ranging from 400 K to 680 K. The 400 K baseline temperature was chosen to be higher than the glass transition temperatures of PDLLA (330 K) to accelerate the sampling procedure.[40] For each hexamer, the molecular structure obtained from the 400 K replica following 50 ns of TIGER2 cycling was saved and then mapped onto a CG structure. After the CG parameters were obtained, TIGER2 simulations using a similar protocol were conducted with the CG models of PDLLA hexamers to further refine the CG parameters until the structure distributions calculated from the CG model optimally matched the corresponding results calculated from the atomistic model.

For the non-bonded terms, the CG parameters were obtained by iterative mapping[24, 25] of the radial distribution functions (RDF) calculated by atomic and CG models of mono-phase systems composed of either D-lactic acid units or L-lactic acid units. The system containing 163 individual lactide units was built in a 25 × 25 × 25 $Å^3$ periodic cube so that the density (1.25 g/cm^3) was similar to that of amorphous PDLLA. We used the CHARMM program to conduct NVT molecular dynamics simulations at 295 K temperature to equilibrate the structure represented by the atomistic and the CG models, respectively, and the last 100 ps trajectory from each simulation was used to calculate the RDF based on the center of mass of each molecule.

2.4. Dry PDLLA

Once the parameters of the CG models of all possible conformers included in the PDLLA chain were optimized for agreement with their respective all-atom models, the CG model of the PDLLA bulk-phase was built and then relaxed with TIGER2/TIGER3. To prepare the starting configuration of the system, a fully extended single chain with chain length 1024 and same amount L and D beads was generated. The positions of the D and L beads were randomly assigned along the chain. Molecular dynamics was carried out with CHARMM at 400 K to relax the chain. A 0.1 kcal/mol harmonic potential was imposed to compress and then constrain all chain segments within a box with dimensions 46.50 × 46.50 × 46.50 $Å^3$. This dimension was set to provide system density of about 1.25 g/cm^3, which was matched to the bulk density of amorphous PDLLA used in this work. Then the single chain was cut evenly into sixteen shorter chains with each chain containing same amount of D and L CG beads (50:50 molar ratio). The harmonic constraint was then removed and the periodic boundary condition was imposed. The model system of PDLLA consisted of sixteen chains with each chain containing sixty-four repeat units, The corresponding molecular weight of each PDLLA chain in the simulation is about 4,600 Da. The structure in the periodic box was then relaxed for 50 ns with the TIGER2/TIGER3 method using eight replicas with temperature levels being evenly distributed between 295 K and 650 K. After obtaining the equilibrated bulk-phase CG structure of the polymer, we selected the lowest energy state from the last 5 ns CG structures and conducted reverse mapping based on the methods presented in ref. 19 to obtain the atomistic bulk-phase model. The recovered structure was energy minimized and equilibrated with the TIGER2 method for 10 ns. The resulted bulk-phase model of PDLLA was validated by comparing the structure factor, $S(q)$, with available experimental result at 295 K. $S(q)$ was theoretically calculated based on the Fourier transform of the total pair distribution function,[41, 42]

$$S(q)=1+4\pi\rho\int_0^\infty r\frac{\sin(rq)}{q}[G^t(r)-1]dr, \quad (4)$$

where r is the distance between atom pairs, ρ is number density, and $G^t(r)$ is the total pair distribution function including the contributions of both intra- and inter-chain atom pairs and was calculated with CHARMM based on the last 10 ps trajectory of each simulation.

2.5. Hydrated PDLLA

Three hydrated PDLLA structures were built with the relaxed structure of PDLLA. The three hydrated PDLLA models labeled as W1, W2, and W3 were built with different weight fractions and initial clustering states of the water (see Table 1). W1 contained 0.56 wt% water whereas W2 and W3 both contained 3.4 wt% water, which were explicitly represented by the PCFF water model.[43] These water weight percentages were based on the experimental data obtained at about day 2 and day 15, respectively. The low concentration of water was chosen because, by the time water content reaches ~ 5%, hydrolysis progresses

to a point where micropores are generated in polymer bulk. The resulting influx of water to these micropores rapidly increases the water content to ~40% between day 10 and day 40. The present simulation is thus an attemptt to capture the structural changes within the polymer before any significant hydrolysis-induced morphological changes occur.

The water molecules were initially distributed in different ways of clustering in the three structures. The different initial conditions of the size of water clusters and the formation of hydrogen bonds for the three simulations are summarized in Table 1, which shows that W3 contains a larger fraction of large water clusters and a smaller fraction of "free" waters (Type 5 water defined in Section 2.6) compared to W1 and W2. To insert water, a TIP3P water box with density 0.994 g/cm^3 was built with same dimension as the dry PDLLA box. The water box was pre-equilibrated at 295 K temperature and then superimposed onto the PDLLA box; the water molecules within the ranges of 2.4 Å (for W1) and 2.0 Å (for W2 and W3) away from the polymer sites were deleted. To adjust the final water content for each system, water molecules were randomly selected and removed until there were 23 waters left in W1 and 148 waters left in W2 and in W3. The simulation box size remained the same as that used for the dry PDLLA calculation, which is reasonable based on Marque et al.'s results that,[44] at concentration at or below ~3 wt%, the water molecules are likely to occupy pre-existing void spaces in the polymer and thus the expansion of the volume of the system is neglectable. The three hydrated structures were relaxed for about 10 ns using the TIGER2 sampling method using eight replicas with temperature levels being evenly distributed between 295 K and 650 K. Based on the TIGER2 trajectory of each simulation, the distribution and clustering of water within the polymer and the interactions between water and PDLLA were studied. The influence of hydration on $S(q)$ was examined in detail and the hydrated models of PDLLA were further validated by comparing the $S(q)$ profiles with experimental measurement at 295 K.

2.6. Hydrogen Bonding

The hydrogen bond (H-bond) pattern within each hydrated PDLLA was analyzed using the SIMULAID program.[45] A H-bond is assumed to form when the distance between a hydrogen atom of a water molecule and an H-bond acceptor in another water molecule or the polymer is less than 2.5 Å and the angle of D (donor) – H ··· A (acceptor) is greater than 90°.[46] Based on the formation of H-bonds, the water molecules were classified into five types: Type 1, waters only H-bonded to carbonyl oxygens on PDLLA; Type 2, waters only H-bonded to ether oxygens on PDLLA; Type3, waters H-bonded to both water molecules and acceptor sites on PDLLA, corresponding the waters linking a water cluster to the polymer; Type 4, waters only H-bonded to other water molecules, referring to clustered waters; and Type 5, "free" waters that are not H-bonded to any acceptor, thus representing isolated water molecules. Table 1 presents the initial distribution of these water types in model systems W1, W2, and W3.

2.7. Physical Behavior of Water

The physical behavior of the water molecules was studied by monitoring the number of H-Bonds between water and the polymer and the size of water clusters (i.e., number of water molecules H-bonded together) within the polymer.

3. Results and Discussion

3.1. Experimental Data

3.1.1. Hydration and Degradation—Both the thermal gravimetric analysis (TGA) and weight measurements showed that the water uptake was small (< 1 wt%) up to about 10 days and then increased to reach a plateau value ~ 40 wt% in about 40 days. The films, that

were transparent to begin with, became opaque and white between 10 to 14 days due to the formation large number of microvoids. The molecular weight began to decrease immediately after the start of the incubation, which reflects polymer chain hydrolysis. However, the degradation appeared to dramatically slowdown after 20 days. Similar results have been reported in the literature.[47, 48] The rapid initial decrease in molecular weight followed by a plateau has been observed even when the media is changed at frequent intervals.[49] Our observation of the change in molecular weight can be explained as follows. The degradation of PDLLA by hydrolytic cleavage of the ester bond starts immediately after the immersion of the specimens in the medium. Initially, degradation follows the gradient in absorbed water, greater near the surface than in the core. During this phase (~ 1-day in our experiment), the degradation products near the surface get dispersed while those in the core remain. This increases the concentration of carboxylic groups in the core, and leads to autocatalysis. After this rapid initial decline in molecular weight, apparent swelling and high influx of water after day 10, the degradation products are solubilized and diffuse out of the polymer, and the entire material is now exposed to the buffer. Absence of autocatalysis in this phase slows down the degradation of the polymer.

3.1.2. X-Ray Scattering—Figure 3 shows the scattering functions of a few representative samples [at t = 0 (dry), 2, 10 and 70 days (wet)] and that of water. The only other data that is available in the literature on PDLLA provides the structure function up to $q = 2.8$ Å^{-1}.[12] In this paper, we provide the results up to $q = 12$ Å^{-1}, and use this data to discuss the details of the water-polymer interactions. The changes in the structure function are small at the 2-day time point, the changes are dramatic at the 10-day time point, and the changes are minimal in samples incubated for longer times. These changes will be interpreted in the following sections. The source of the shoulder at 0.4 Å^{-1} seen in all the wet samples is yet to be understood.

3.2. Coarse-Grained Model of PDLLA

The parameterization of the CG model of PDLLA was carried out based on the 50 ns TIGER2 trajectories of the atomistic simulations for a system composed of PDLLA hexamers (see details in the supplementary materials). The optimized CG parameter for $E_{stretch}$, E_{bend}, $E_{torsion}$, and E_{VDW} terms are summarized in Tables S2 – S5 respectively. The mapping of the distributions of bond lengths, bond angles, dihedral angles, and RDFs calculated by the CG model of PDLLA onto the corresponding distributions calculated by the atomistic model of PDLLA are shown in Figures S1 – S4, respectively.

It is noted that the mapping between the profiles calculated with CG and atomistic models may deviate when temperature changes. Since in the TIGER2/TIGER3 algorithm the purpose of using higher temperatures is only to rapidly move around the conformational phase space, deviations of the molecular behavior from the CG parameters at the elevated temperatures is not important. However, because results from 400 K simulations are used to set the CG parameters, which are then considered to represent the polymer's behavior at 295 K, additional calculations were conducted at 295 K and 680 K temperature levels based on the atomistic model of E1DDDLE2 hexamers for comparison to 400 K behavior. Examples of the results of these simulations (probability profiles of bond length, bond angle, and dihedral angles) are presented in Figure S5 (A) – (C) at 295 K and 680 K temperatures together with the corresponding results at 400 K temperature. In general, when compared to the 400 K temperature results that were used in mapping the CG profiles, the 295 K profiles are very consistent with the 400 K profiles. On the other hand, the 680 K profiles exhibit substantially differences in the peak height of the profiles, with the location of peak positions being generally the same.

3.3. Dry PDLLA

The bulk-phase model of dry PDLLA consisted of 16 chains with each chain having 64 repeat units. The system represented by CG model was equilibrated with the TIGER2/TIGER3 method for 50 ns, which was considered to be sufficiently long to establish a well–equilibrated ensemble (The potential energy of the system was observed to stabilize to an apparent minimum value after only about 5 ns). We then selected the lowest energy state from the last 5 ns trajectory and conducted reverse mapping to obtain the atomistic structure of PDLLA. The recovered structure was energy minimized and equilibrated with TIGER2 for 10 ns. To examine whether the recovered atomistic structure is a reasonable representative of the equilibrium bulk-phase of actual PDLLA, we calculated the structure function, $S(q)_{\mathrm{dry}}$, based on the last 100 ps trajectory of the 295 K replica and compared it with that measured by x-ray diffraction. Figure 4(A) compares the experimental and simulation results of $S(q)_{\mathrm{dry}}$. The positions of the main peaks predicted by simulation agree very well with those measured experimentally over the entire range of q, indicating that the atomistic model realistically contains each of the primary structural features of amorphous PDLLA. In addition, Figure 5(B – D) presents in thin lines the calculated partial structure functions $S(q)_{\mathrm{dry}}^{\mathrm{C-C}}$, $S(q)_{\mathrm{dry}}^{\mathrm{O-O}}$, and $S(q)_{\mathrm{dry}}^{\mathrm{C-O}}$, respectively, with which it can be specified that, in the calculated $S(q)_{\mathrm{dry}}$ (Figure 5A), the peaks located at $q = 1.2$ Å^{-1} and 5.8 Å^{-1} are mainly attributed to C–C and C–O correlations and the two peaks located between $q = 2$ to 3 Å^{-1} are mainly related to O–O correlation. The presence of the peak at $q = 1.5$ Å^{-1} in the $S(q)_{\mathrm{dry}}^{\mathrm{C-C}}$ profile accounts for the shoulder around the same position in $S(q)_{\mathrm{dry}}$.

3.4. Hydrated PDLLA

3.4.1. Structure Functions—The hydrated PDLLA systems, W1, W2, and W3, were equilibrated with TIGER2 for 10 ns. Figure 6 presents a representative configuration of W3 after 10 ns equilibration. Based on the last 100 ps trajectory of the 10 ns TIGER2 cycling at 295 K, the profiles of $S(q)$ were calculated for W1, W2, and W3 and the results are presented together with that of dry PDLLA in Figure 4(B). As shown in this figure, W2 and W3, which started with the same net concentration of water (3.4 wt%) but with different initial distributions of water within the polymer (see Table 1), obtained converged results of $S(q)$. The profiles of $S(q)$ obtained from W1 (Green), W2 (Magenta) and W3 (Blue) tend to deviate from the calculated $S(q)_{\mathrm{dry}}$, (Red), and the deviations are presented in both the height and position of some of the main peaks and these changes are consistent with the trend observed in the experimental studies (Figure 3). Specifically, compared to $S(q)_{\mathrm{dry}}$, the peaks of the $S(q)$ profiles for the hydrated PDLLA, located at $q = 1.2$ Å^{-1} and 5.8 Å^{-1} decreased whereas the height of the two peaks located between $q = 2$ to 3 Å^{-1} increased, and the positions of the peaks between $q = 2$ to 3 Å^{-1} shifted toward smaller q.

Figure 4(C) compares the profile of $S(q)$ obtained from the W3 simulation with the observation result for the two-day hydrated PDLLA. The profiles of $S(q)$ of bulk water obtained from simulation and experiment are also displayed in Figure 4(C). Again, it is observed that the W3 result agrees very well with the measured result for hydrated PDLLA. Moreover, for the bulk water, the simulation result based on the PCFF water model is also in excellent agreement with the experimental data as well as with the previous calculation results based on different water models.[51] Since the water–water correlation results in strong peaks between $q = 2$ to 3 Å^{-1}, the addition of water to the dry system of PDLLA caused the shifts of the two peaks located between $q = 2$ to 3 Å^{-1} in the profiles of $S(q)$ in both experiment and simulation for hydrated systems.

The contribution of water to the total $S(q)$ of hydrated PDLLA can be decomposed into three parts, i.e., water–water correlation, water–polymer correlation, and the corresponding

changes of positional order of PDLLA sites due to the presence of water. To specify the influence of water–polymer interactions on the total $S(q)$, we calculated the partial structure functions $S(q)_{W3}^{C-C}$, $S(q)_{W3}^{O-O}$, and $S(q)_{W3}^{C-O}$ for W3 and plotted the results in Figure 5(B – D) together with the corresponding results obtained from dry PDLLA. The total $S(q)_{W3}$ was also plotted together with $S(q)_{dry}$ in Figure 5(A). Again, it is observed that the O–O pair correlation caused the increases of the height of the peaks in the range of $q = 2$ to 3 $Å^{-1}$ in $S(q)_{W3}^{O-O}$. When the contributions of polymer–water and water–water interactions to $S(q)_{W3}^{O-O}$ were considered separately, we found that, in W3 with about 3.4 wt% water, the polymer–water interaction attributed about 95% to the peak height and the water–water interaction attributed about 5% to the peak height with respect to $S(q)_{dry}^{O-O}$. Other main changes are the decreases of the height of the $S(q)^{C-O}$ peak at $q = 1.2$ $Å^{-1}$ and the peak for $S(q)_{W3}^{C-C}$ at $q = 1.5$ $Å^{-1}$, which leads to the corresponding decrease of the peak height in the range of $q = 1.2 – 1.6$ $Å^{-1}$ in $S(q)_{W3}$.

For C–C, C-O and O–O pairs, we also calculated their radial distribution functions, $g(r)^{C-C}$, $g(r)^{C-O}$ and $g(r)^{O-O}$, which characterize the positional order of the atom pairs and determine the behavior of the corresponding partial structure functions before and after hydration. In the result of $g(r)^{C-C}$ presented in Figure 7(A), the first peak around $r = 1.54$ Å was created by the carbon atom pairs connected by covalent bond (see Figure 2) and the rest of the peaks at larger distances correspond to the positional correlation of non-bonded carbon atom pairs. Compared to the result of the dry sample (thin line), the heights of the main peaks in the hydrated structure (thick line) decrease slightly, but the positions of these peaks remain unchanged. The reduction of the peak height is attributed to the decrease of carbon concentration due to the addition of water. In all hydrated systems studied in this work, since the concentration of water is low and the void space among the polymer segments was sufficient to accommodate the water molecules, the space occupation of water did not change the positional order of non-bonded carbon atom pairs.

In the profiles of $g(r)^{C-O}$ given in Figure 7(B), the first three peaks located at about $r = 1.2$, 1.4 and 2.45 Å were created by the atom pairs of bonded $C\alpha=O_1$, $C\alpha–O_2$ (see Figure 2) in the ester group and non-bonded neighboring C_β and O_1. The peaks beyond $r = 2.5$ Å were due to non-bonded C–O pairs. When compared to the profile of dry PDLLA (thin line), it is observed that, in the profile of hydrated structure (thick line), the heights of the peaks caused by the bonded C–O pairs slightly decreased and the heights of the peaks caused by the non-bonded C–O pairs slightly increased. The increase of the heights of the peaks attributed to non-bonded C–O interactions is an indication that the water molecules are distributed around the ester groups in the hydrated structure.

In the result of $g(r)^{O-O}$ presented in Figure 7(C), the first peak around $r = 2.3$ Å was created by the oxygen atom pairs within same ester functional group (see Figure 2), and the two peaks located at about $r = 3$ Å and 3.6 Å were created by non-bonded oxygen atom pairs. The non-bonded oxygen atom pairs come from not only polymer segments in dry PDLLA, with additional contributions from water–polymer and water–water interactions in the hydrated PDLLA. Compared to the $g(r)^{O-O}$ of dry PDLLA, several changes are observed in the $g(r)^{O-O}$ of hydrated PDLLA. The height of the first peak decreased while its position remained the same. This is attributed to the decrease of the concentration of ester groups due to the addition of water; the two peaks located at about $r = 3$ Å and 3.6 Å shift toward smaller r with increasing peak height. This suggests that distances > 3 Å are more populated in the wet sample, and indicate that, in the structure of hydrated PDLLA, the water molecules are closely distributed around the ester groups and thus change the positional order of O–O atom pairs. Based on the criterion of H-bond formation,[46] an H-bond may be formed if the distance between a hydrogen donor and acceptor is smaller than 3.9 Å.

Therefore, the changes in $g(r)^{O-O}$ suggest the waters around the ester groups may form H-bonds with the carbonyl or the ether oxygen. Furthermore, the shift of the positions of these peaks toward the position of the water O–O peak (the insert of Figure 7(C) gives the $g(r)^{O-O}$ of pure water, which shows strong positional correlation around distance 2.8 Å) suggests the presence of water clusters in the system.

3.4.2. Hydrogen Bonding—The results presented in Figures 8 and 9 show an analysis of the trajectories for W1, W2, and W3 simulations indicated that the average number of H-bond between the water and the polymer, and the fractions of various types of water cluster, fluctuated in the early stage of simulation and gradually reached plateau values after 6 ns of sampling time. Using the trajectories after 6 ns, we calculated the percentage of water in various sizes of water clusters (Figure 8). The water clusters were classified based on their size, which was determined by the number of H-bonded water molecules within the cluster. The smallest cluster contained only an individual water molecule. Figure 8 shows that the systems with a higher concentration of water (W2 and W3; 3.4 wt% water) contained higher fractions of large-size water clusters and a lower fraction of individual water molecules compared to the W1 system (0.56 wt% water). In the equilibrated W1, W2, and W3 structures, the largest clusters contained 2, 7, and 10 molecules, respectively. Furthermore, the largest number of H-bonds formed between the water and the polymer in W3, which contained the higher concentration of water and the largest size of initial water clusters. Using the last 4 ns trajectory of each simulation, we also calculated the average percentage of each type of water (i.e., Types 1 – 5) for each of our three simulated systems (i.e., W1, W2, and W3) and present the results in Figure 9. These analyses show a similar trend in the distribution of the water types for each of our three systems, with Type 1 water (H-bonded to carbonyl oxygen) and Type 5 water (isolated water molecules) being the predominate water types in each system. In all calculated structures, the ratio of H-bonds formed between water and carbonyl oxygen (Type 1) to that formed between water and ether oxygen (Type 2) is more than 4:1. Since the molar ratio of carbonyl oxygen to ether oxygen is 1:1 in PDLLA, it can be concluded that in hydrated PDLLA, the carbonyl oxygen is more accessible to water than the ether oxygen.

Figure 10 compares the structure functions calculated for bulk water ($S(q)_{\text{bulk-wat}}$) and the water distributed in the hydrated PDLLA (W3, $S(q)_{\text{W3-wat}}$) at 295 K temperature, considering only the water-water contributions (i.e., excluding water-polymer contributions) to the structure function. To calculate the structure function, the density of the water in W3 was rescaled by the factor of N_{tot}/N_{wat}, where N_{tot} is the number of total atoms in W3 and N_{wat} is the number of atoms in water in W3. The overall profiles of $S(q)_{\text{bulk-wat}}$ and $S(q)_{\text{W3-wat}}$ are similar, indicating that the organization of water molecules in the clusters in W3 is similar to that in the bulk water. However, due to the fact that the water clusters in W3 were absorbed within the polymer by forming H-bonds with the oxygen atoms in the ester groups, similar to the observations for water confined in hydrophilic media,[52] the structure of the water layers adjacent to the polymer is distorted from the ordered organization in bulk water. In $S(q)_{\text{bulk-wat,}}$ the main peaks located in the range of $q = 2.0$ to 6.0 $Å^{-1}$ characterize the short-range tetrahedral ordering in bulk water.[51] The partially distorted structure of the water clusters led to the decrease of the heights of these peaks in $S(q)_{\text{W3-wat}}$.

3.4.3. Application of the TIGER2/TIGER3 Sampling Method and Its Computational Cost—The results of these studies demonstrate that the molecular simulations using the TIGER2/TIGER3 method were successfully able to provide very reasonable molecular-level insights that assist in explaining the experimentally observed results. This sampling method has been tested by a variety of distinctly different molecular systems[16–19] and found to provide Boltzmann-weighted ensembles of sampled states very

similar to conventional REMD simulations for each of these systems if the sampling procedure is properly applied. Guidance on how to set up the simulation protocol to properly perform a TIGER2/TIGER3 simulation is provided in ref 18. As demonstrated in the present study, the TIGER2/TIGER3 method is particularly well suited for the simulation of entangled long chain molecular systems, with TIGER2 alone being particularly well suited for the simulation of molecular systems that are generally considered to be too large (and thus computationally costly) to be handled by a conventional REMD simulation.

The computational time required for the TIGER2/TIGER3 method for a given total amount of simulated time is comparable to the time required to perform a conventional REMD simulation. For instance, the dry PDLLA system required 50 ns of sampling time to produce an equilibrated ensemble of states using the CG model, which was composed of 5,000 TIGER2/TIGER3 cycles. On average, each cycle takes about 1.2 minutes CPU time on Clemson Palmetto cluster with 2.33 GHz processors, with 50 ns of sampling thus requiring a total of 100 hours CPU time.

3.4.4. Approaches to Study Hydrolysis and Degradation—This present work was focused on predicting the distribution of water within the polymer, thus the effects of hydrolysis and polymer degradation were not considered. However, hydrolysis and degradation are important processes in hydrated polymers. The process of degradation may be addressed in several ways. The simplest way would be to randomly break chains, cap the ends with carboxylate groups, and then evaluate how this influences water distribution within the polymer. More complex approaches would be to use either a bond-breaking molecular mechanics (MM) potential, or to conduct combined quantum mechanics and molecular mechanics (QM/MM) simulations,[53] with the QM part focusing on the areas of the polymer where water is predicted by the TIGER2 simulations to be clustered. This could then involve iterative simulations of QM/MM followed by further simulations using TIGER2/TIGER3 to re-equilibrate the water within the polymer after the hydrolysis steps.

4. Conclusion

The TIGER2/TIGER3 scheme was able to greatly accelerate the relaxation of dense, entangled amorphous polymer systems. In this mixed sampling scheme, the TIGER3 algorithm enables the system configuration to rapidly change by allowing the chain segments to freely pass through one another, while the TIGER2 algorithm is used to efficiently relax and re-equilibrate the system following the TIGER3 process to eliminate effects caused by chain overlaps. In this work, the TIGER2/TIGER3 was implemented to generate equilibrium amorphous structure of PDLLA represented by a CG model. The atomic representation of the equilibrated amorphous polymer was then obtained by translating the CG model back with reverse-mapping. This was validated by the excellent agreement between the simulation and experimental results for $S(q)$ over a large range of q values (i.e., from 0.5 to 10 $Å^{-1}$).

Based on the carefully prepared bulk-phase model of PDLLA, three hydrated PDLLA models were generated and relaxed using the TIGER2 sampling method. Studies based on the relaxed hydrated structures reveal the properties of water presented in the polymer network. The H-bonds formed between water molecules result in the formation of water clusters and the H-bonds formed between water and acceptor sites on polymer account for attaching the water molecules or their clusters to the polymer. The H-bond acceptors on polymer include both carbonyl oxygen and ether oxygen. The simulation results indicated that the carbonyl oxygen is much more accessible to water than the ether oxygen. The H-bonding interactions cause the water molecules to be closely distributed around the ester

functional groups in PDLLA, thus leading to a different positional order of O–O atom pairs and corresponding changes in the profiles of $S(q)$ for hydrated PDLLA.

Supplementary Material

Refer to Web version on PubMed Central for supplementary material.

Acknowledgments

Financial support for this work was provided by RESBIO, a Research Resource funded by the National Institutes of health under NIH grant EB001046, the New Jersey Center for Biomaterials, and Rutgers University. We also acknowledge the contributions of Dr. Pradip Biswas, Tougaloo College, Tougaloo, MS for modifications to the CHARMM code to enable the use of the PCFF force field for polymer simulations. The x-ray scattering work was carried out at the advanced photon source (APS), Argonne National Laboratory (ANL) which is supported by the U.S. Department of Energy. We thank Mr. Barry Cunningham for water uptake and molecular weight measurements, Dr. Yang Ren for assisting in the data collection at ANL-APS beamline 11-ID-C, Dr. Chris Benmore for discussion regarding data analysis, and Dr. Lawrie Skinner for permission to use the water scattering data.

References and Notes

1. Barrows TH. Clin Mater. 1986; 1:233–257.
2. Brocchini J, James K, Tangpasuthadol V, Kohn J. J Biomed Mater Res. 1998; 42:66–75. [PubMed: 9740008]
3. Chandra R, Rustgi R. Prog Polym Sci. 1998; 23:1273–1335.
4. Middleton JC, Tipton AJ. Biomater. 2000; 21:2335–2346.
5. Kumar N, Ravikumar MN, Domb AJ. Adv Drug Delivery Rev. 2001; 53:23–44.
6. Formin VA. Prog Rubber Plast Technol. 2001; 17:186–204.
7. Holten, CH. Lactic Acid. Verlag Chemie; Berlin: 1971.
8. Li S, Garreau H, Vert M. J Mater Sci Mater Med. 1990; 1:198–206.
9. Li S, Vert M. Macromolecules. 1994; 27:3107–3110.
10. Siparsky GL, Voorhees KJ, Dorgan JR, Schilling K. J Environ Polym Degr. 1997; 5:125–136.
11. Blomqvist J, Mannfors B, Pietilä LO. Polymer. 2002; 43:4571–4583.
12. Entrialgo-Castaño M, Lendlein A, Hofmann D. Adv Eng Mater. 2006; 8:434–439.
13. Entrialgo-Castaño M, Salvucci AE, Lendlein A, Hofmann D. Macromol Symp. 2008; 269:47–64.
14. Hofmann D, Entrialgo-Castaño M, Kratz K, Lendlein A. Adv Mater. 2009; 21:3237–3245. [PubMed: 20882494]
15. Gautieri A, Mezzanzanica A, Motta A, Redealli A, Vesentini S. J Mol Model. 2012; 18:1495–1502. [PubMed: 21785936]
16. Li X, Murthy NS, Latour RA. Macromolecules. 2011; 44:5452–5464. [PubMed: 21769156]
17. Li X, Latour RA, Stuart SJ. J Chem Phys. 2009; 130:174106: 1–9. [PubMed: 19425768]
18. Li X, Latour RA. J Comput Chem. 2011; 32:1091–1100. [PubMed: 20949510]
19. Li X, Latour RA. Polymer. 2009; 50:4139–4149. [PubMed: 20161121]
20. Tschöp W, Kremer K, Batoulis J, Bürger T, Hahn O. Acta Polymer. 1998; 49:61–74.
21. León S, van der Vegt N, Delle Site L, Kremer K. Macromolecules. 2005; 38:8078–8092.
22. Hess B, León S, van der Vegt N, Kremer K. Soft Matter. 2006; 2:409–414.
23. Srinivas G, Discher DE, Klein ML. Nature Mater. 2003; 3:638–644. [PubMed: 15300242]
24. Reith D, Meyer H, Müller-Plathe F. Macromolecules. 2001; 34:2335–2345.
25. Milano G, Goudeau S, Müller-Plathe F. J Polym Sci: Part B: Polym Phys. 2005; 43:871–885.
26. Hammersley, AP. FIT2D V10.3 Reference Manual V4.0. European Synchrotron Radiation Facility; 1998.
27. Thompson JW, Billinge SJL. J Appl Cryst. 2004; 37:678–678.

28. Metropolis N, Rosenbluth AW, Rosenbluth MN, Teller AH, Teller E. J Chem Phys. 1953; 21:1087–1092.
29. Brooks BR, Bruccoleri RE, Olafson BD, States DJ, Swaminathan S, Karplus M. J Comput Chem. 1983; 4:187–217.
30. MacKerell AD, Bashford D, Bellott M, Dunbrack RL, Evanseck JD, Field MJ, Fischer S, Gao J, Guo H, Ha S, Joseph-McCarthy D, Kuchnir L, Kuczera K, Lau FTK, Mattos C, Michnick S, Ngo T, Nguyen DT, Prodhom B, Reiher WE, Roux B, Schlenkrich M, Smith JC, Stote R, Straub J, Watanabe M, Wiorkiewicz-Kuczera J, Yin D, Karplus M. J Phys Chem B. 1998; 102:3586–3616.
31. Andersen HC. J Chem Phys. 1980; 72:2384–2393.
32. Nosé S. Mol Phys. 1984; 52:255–268.
33. Hoover WG. Phys Rev A. 1985; 31:1695–1697. [PubMed: 9895674]
34. Allen, M.; Tildesly, D. Computer Simulation of Liquids. Oxford University Press; Oxford: 1991.
35. Hariharan PC, Pople JA. Theor Chim Acta. 1973; 28:213–222.
36. Francl MM, Pietro WJ, Hehre WJ, Binkley JS, Gordon MS, DeFrees DJ, Pople JA. J Chem Phys. 1982; 77:3654–3665.
37. Dinur, U.; Hagler, AT. Reviews in Computational Chemistry. Lipkowitz, KB.; Boyd, DB., editors. Vol. 2. VCH Publishers; New York: 1991. p. 99-164.
38. Maple JR, Hwang MJ, Stockfisch TP, Dinur U, Waldman M, Ewig CS, Hagler AT. J Comp Chem. 1994; 15:162–182.
39. Blomqvist J, Mannfors B, Pietilä LO. J Mol Struct. 2000; 531:359–374.
40. Chen C, Depa P, Maranasa JK. J Chem Phys. 2008; 128:124906. [PubMed: 18376972]
41. Mavrantzas VG, Boone TD, Zervopoulou E, Theodorou DN. Macromolecules. 1999; 32:5072–5096.
42. Keen DA. J Appl Cryst. 2001; 34:172–177.
43. Fritz L, Hofmann D. Polymer. 1997; 38:1035–1045.
44. Marque G, Neyertz S, Verdu J, Prunier V, Brown D. Macromolecules. 2008; 41:3349–3362.
45. Mezei M. J Comp Chem. 2003; 31:2658–2668. [PubMed: 20740566]
46. McDonald IK, Thornton JM. J Mol Biol. 1994; 238:777–793. [PubMed: 8182748]
47. Dorati R, Genta I, Colonna C, Modena T, Pavanetto F, Perugini P, Conti B. Polym Degrad Stabil. 2007; 92:1660–1668.
48. Zheng XT, Zhou SB, Yu XJ, Li XH, Feng B, Qu SX, Weng J. J Biomed Mater Res Part B: Appl Biomater. 2008; 86B:170–180. [PubMed: 18161831]
49. Ali SAM, Doherty PJ, Williams DF. J Biomed Mat Res. 1993; 27:1409–1418.
50. Humphrey W, Dalke A, Schulten K. J Mol Graphics. 1996; 14:33–38.
51. Wikfeldt KT, Leetmaa K, Ljungberg MP, Nilsson A, Pettersson LG. J Phys Chem B. 2009; 113:6246–6255. [PubMed: 19358575]
52. Mancinelli R, Imberti S, Soper AK, Liu KH, Mou CY, Bruni F, Ricci MA. J Phys Chem B. 2009; 113:16169–16177. [PubMed: 19928867]
53. Zhang R, Lev B, Cuervo JE, Noskov SY, Salahub DR. Adv Quantum Chem. 2010; 59:353–400.

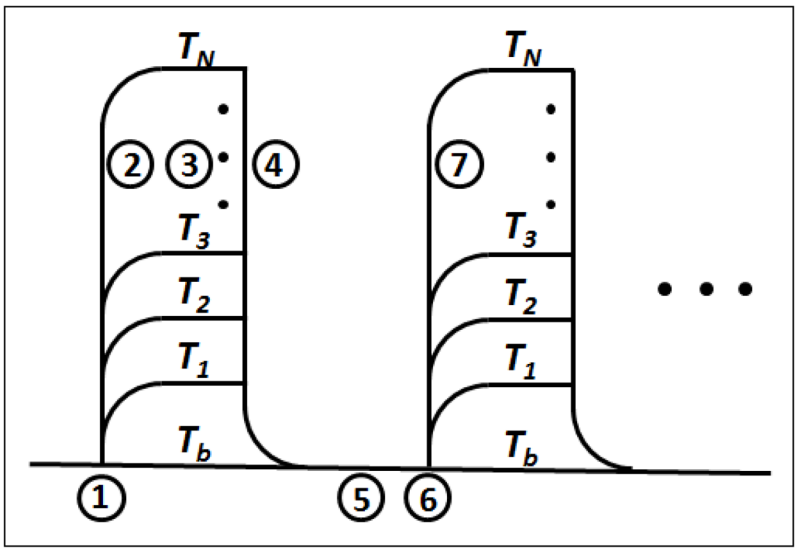

Figure 1.

A schematic representation of the TIGER2/TIGER3 algorithm. TIGER2: (1) A set of N+1 replicas are assigned to temperatures ranging from T_b (baseline temperature of interest) to T_N with uniform separation between temperature levels. (2) Replicas assigned to elevated temperatures are rapidly heated by velocity rescaling. (3) Replicas are equilibrated at each assigned temperature. (4) Replicas are rapidly quenched by velocity rescaling to T_b, and (5) equilibrated at T_b. (6) One quenched replica is randomly selected and its potential energy is compared with that of the baseline replica using the Metropolis criterion. If the Metropolis criterion is satisfied, the selected high temperature replica is added to the sampled ensemble of states and reassigned to T_b. If not, the baseline replica is added to the ensemble and reassigned to T_b for the next cycle. Replicas not reassigned to T_b are then assigned to the elevated temperature levels based on their potential energies, with the highest potential energy being assigned to T_N. A TIGER3 cycle is similar to TIGER2, except the radii of the CG beads for the replicas assigned to the higher temperature are reduced to zero to allow chain segments to pass through one another. As part of step (3), the beads are then regrown in size, the systems are energy minimized, and then re-equilibrated to their designated elevated temperature level prior to quenching back down to T_b.

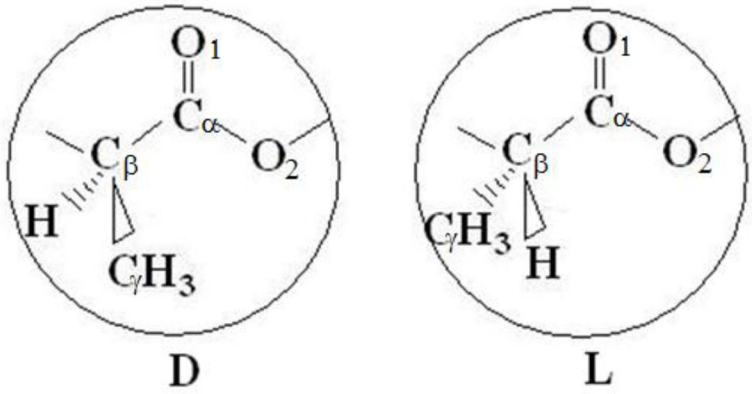

Figure 2.
Schematic representations of the atomic and the CG models for D-lactic acid and L-lactic acid.

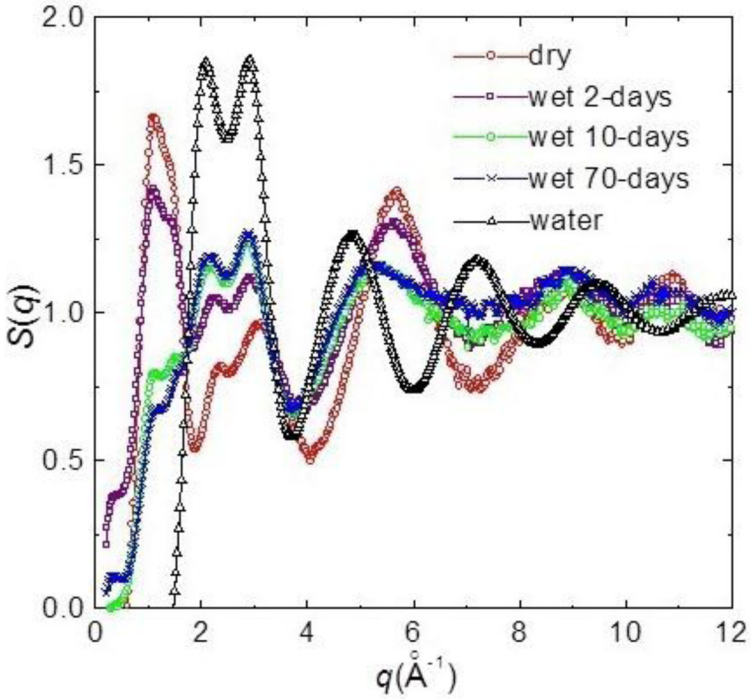

Figure 3.
Experimental observations of the 295 K scattering functions of water (black triangle), dry sample (red circle), and wet samples in two (purple square), ten (green circle) and seventy (blue cross) days.

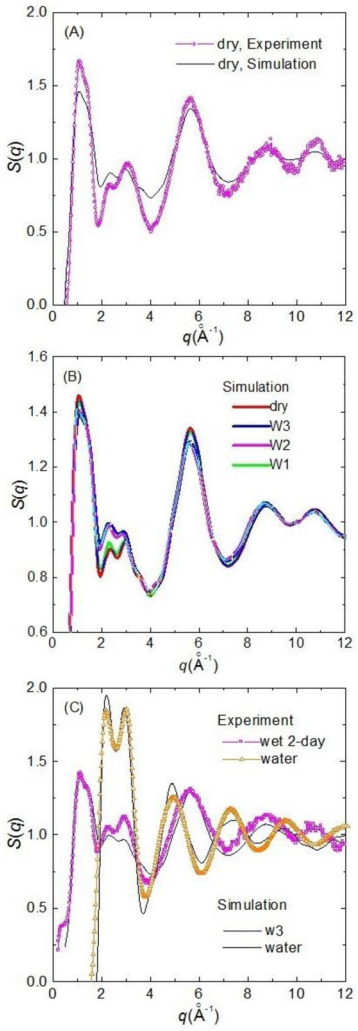

Figure 4.

(A) Comparison of the experimental (Magenta) and simulation (Blue) results of structure function for dry PDLLA at 295 K temperature. (B) Comparison of the structure functions at 295K temperature calculated for dry PDLLA (Red) and three hydrated PDLLA systems, W1 (Green), W2 (Magenta), and W3 (Blue). (C) Comparisons of the two-day experimental (Magenta) and the W3 simulation (Blue) results of structure function for hydrated PDLLA at 295 K temperature, and the experimental (Orange) and simulation (Black) results of structure function for bulk water.

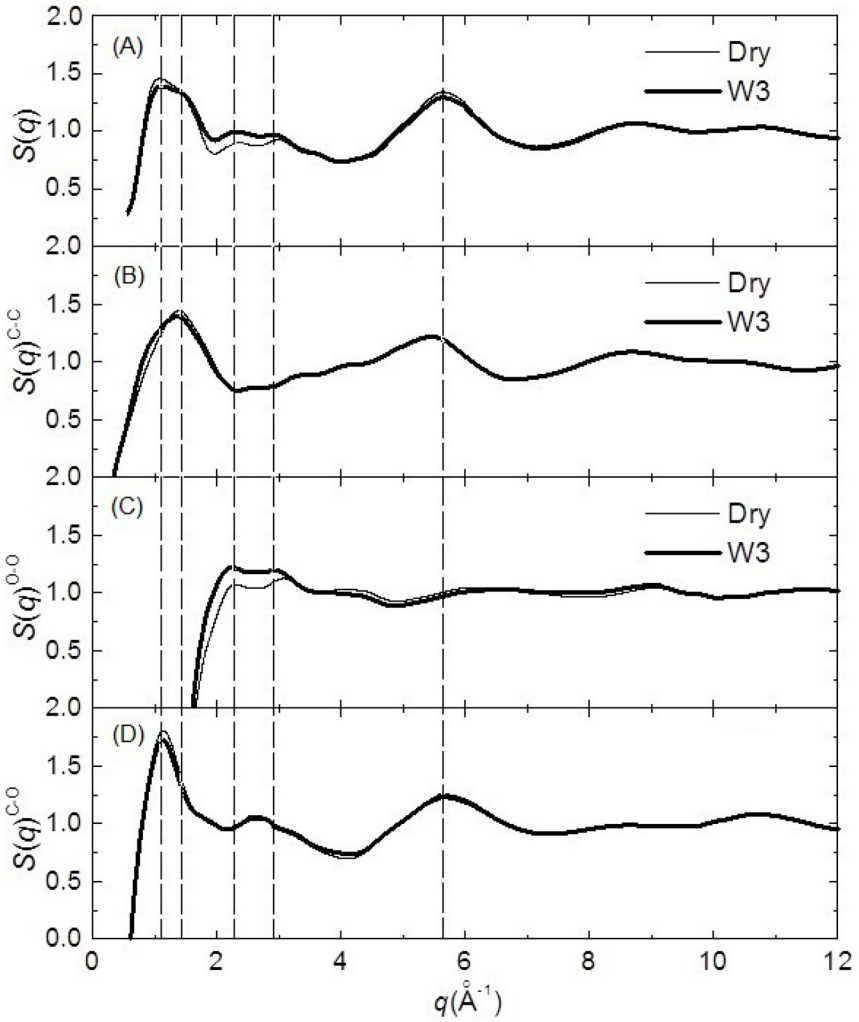

Figure 5.

Comparisons of (A) the total structure functions of dry (thin line) and hydrated (thick line) PDLLA obtained from W3 simulation at 295 K, and the partial structure functions (B) $S(q)^{C–C}$, (C) $S(q)^{O–O}$, and (D) $S(q)^{C–O}$ obtained from simulations for dry (thin line) and hydrated (W3, thick line) PDLLA at 295 K.

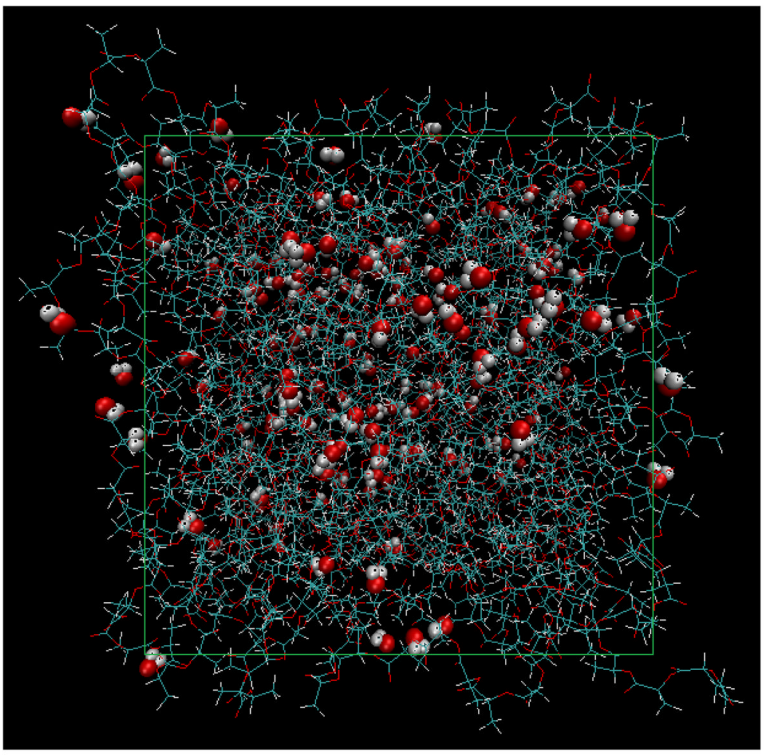

Figure 6.
A representative equilibrated W3 structure. The plot was created with VMD program.[50]

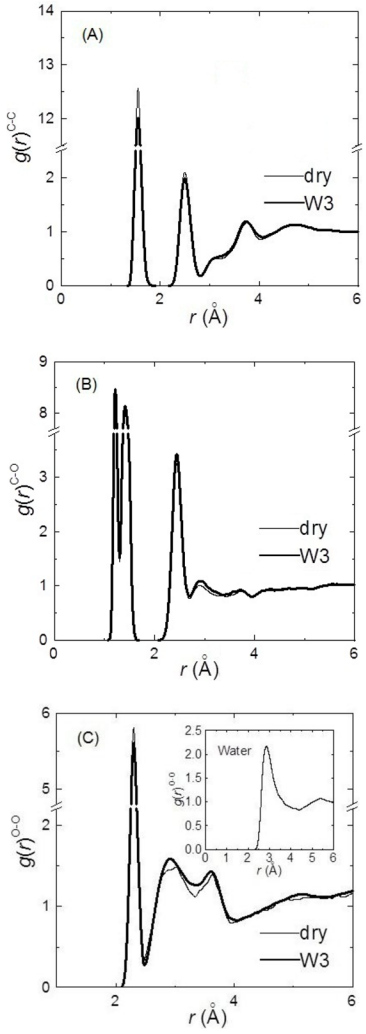

Figure 7.

Comparisons of partial radial distribution functions, (A) $g(r)^{C-C}$, (B) $g(r)^{C-O}$, and (C) $g(r)^{O-O}$ calculated for dry (thin line) and hydrated (W3, thick line) PDLLA. The insert in (C) is the $g(r)^{O-O}$ of bulk water.

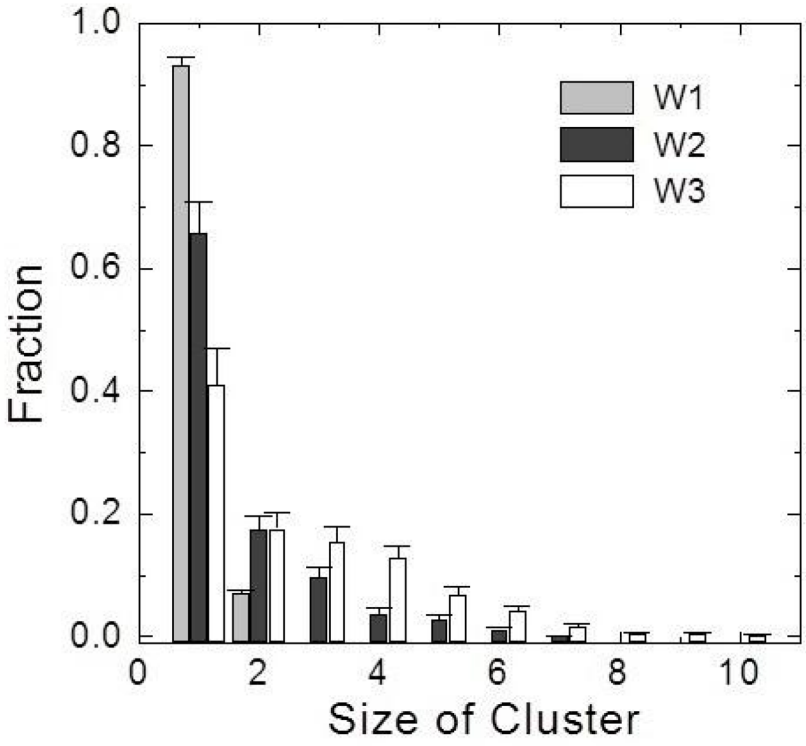

Figure 8.
Average fractions of water clusters of different size over the last 4ns TIGER2 simulations for W1 (Grey), W2(Black), and W3 (White) systems.

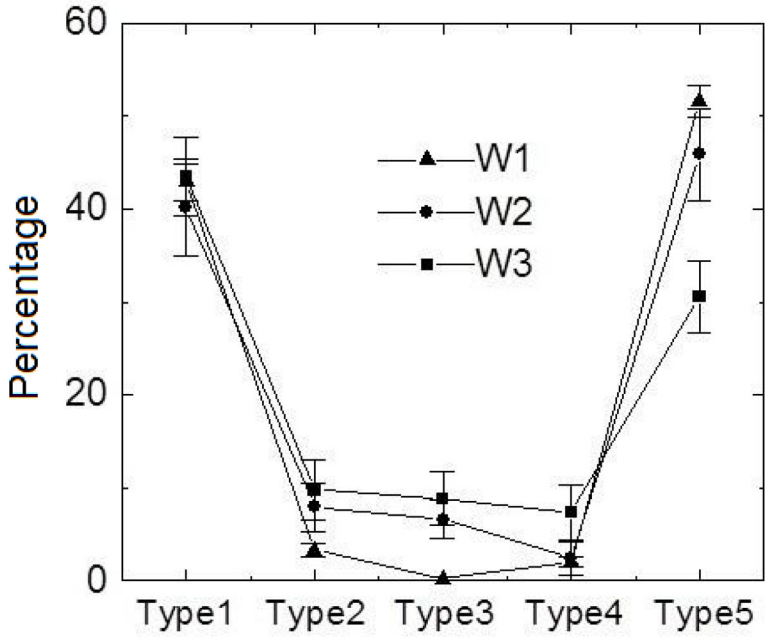

Figure 9.
The percentages of five types of water molecules calculated based on the last 4 ns TIGER2 simulations for W1 (Triangle), W2(Circle), and W3 (Square) systems.

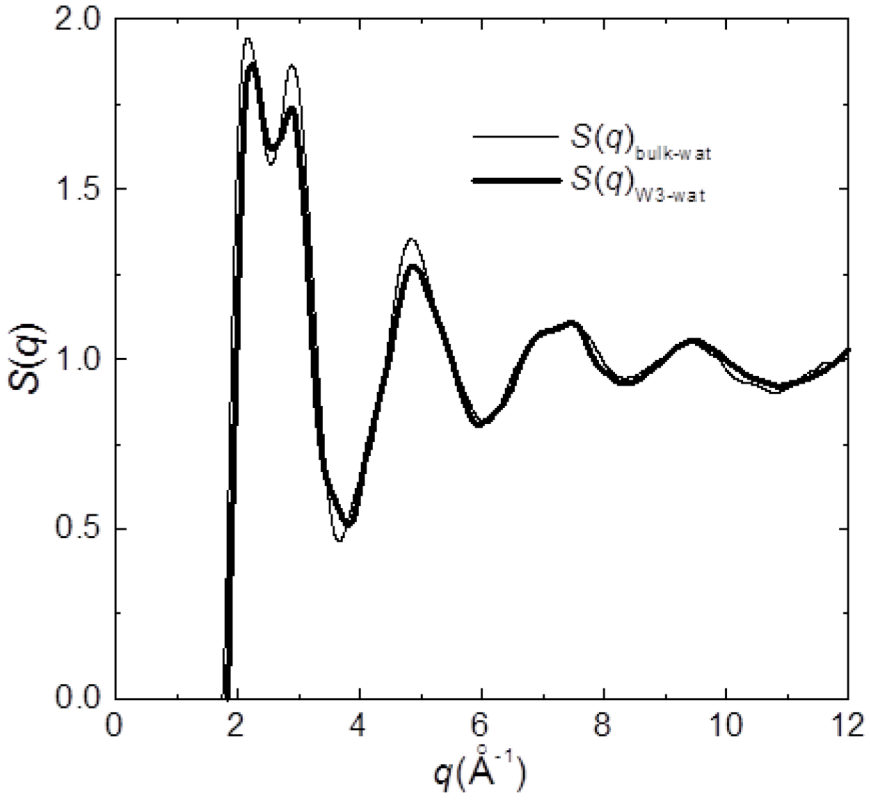

Figure 10.
Comparison of the structure functions of bulk water, $S(q)_{\text{bulk-wat}}$ (thin line), and the water distributed in W3 system, $S(q)_{\text{W3-wat}}$ (thick line).

Table 1

The percentage of water contained in different size of water clusters ([a]) and in five types of water ([b]) in the initial structure of W1, W2, and W3 simulations.

Index [c]	Simulation W1		Simulation W2		Simulation W3	
	Percentage [a]	Percentage [b]	Percentage [a]	Percentage [b]	Percentage [a]	Percentage [b]
1	91.30	60.86	66.89	39.19	27.70	37.12
2	8.70	0.00	18.92	10.14	18.92	18.28
3	0	4.35	8.11	6.08	14.19	6.76
4	0	4.35	2.70	1.35	10.81	14.54
5	0	30.44	3.38	43.24	13.51	23.30
6	0		0		8.11	
7	0		0		0	
8	0		0		0	
9	0		0		0	
10	0		0		6.76	

[c]The index refers to the size of water cluster when ([a]) is considered and refers to the type of water when ([b]) is considered.

Macromolecules. Author manuscript; available in PMC 2013 June 12.